# Rangeland hydrology and erosion model (RHEM) enhancements for applications on disturbed rangelands

Osama Z. Al-Hamdan,[1,2]* Mariano Hernandez,[3,4] Frederick B. Pierson,[1] Mark A. Nearing,[3] C. Jason Williams,[1] Jeffrey J. Stone,[3] Jan Boll[2] and Mark A. Weltz[5]

[1] *Northwest Watershed Research Center, USDA, Agricultural Research Service, Boise, ID, USA*
[2] *Department of Biological and Agricultural Engineering, University of Idaho, Moscow, ID, USA*
[3] *Southwest Watershed Research Center, USDA, Agricultural Research Service, Tucson, AZ, USA*
[4] *School of Natural Resources and Environment, University of Arizona, Tucson, AZ, USA*
[5] *USDA, Great Basin Rangelands Research Unit, Reno, NV, USA*

## Abstract:

The rangeland hydrology and erosion model (RHEM) is a new process-based model developed by the USDA Agricultural Research Service. RHEM was initially developed for functionally intact rangelands where concentrated flow erosion is minimal and most soil loss occurs by rain splash and sheet flow erosion processes. Disturbance such as fire or woody plant encroachment can amplify overland flow erosion by increasing the likelihood of concentrated flow formation. In this study, we enhanced RHEM applications on disturbed rangelands by using a new approach for the prediction and parameterization of concentrated flow erosion. The new approach was conceptualized based on observations and results of experimental studies on rangelands disturbed by fire and/or by tree encroachment. The sediment detachment rate for concentrated flow was calculated using soil erodibility and hydraulic (flow width and stream power) parameters. Concentrated flow width was calculated based on flow discharge and slope using an equation developed specifically for disturbed rangelands. Soil detachment was assumed to begin with concentrated flow initiation. A dynamic erodibility concept was applied where concentrated flow erodibility was set to decrease exponentially during a run-off event because of declining sediment availability. Erodibility was estimated using an empirical parameterization equation as a function of vegetation cover and surface soil texture. A dynamic partial differential sediment continuity equation was used to model the total detachment rate of concentrated flow and rain splash and sheet flow. The enhanced version of the model was evaluated against rainfall simulation data for three different sites that exhibit some degree of disturbance by fire and/or by tree encroachment. The coefficient of determination ($R^2$) and Nash–Sutcliffe efficiency were 0.78 and 0.71, respectively, which indicates the capability of the model using the new approach for predicting soil loss on disturbed rangeland. By using the new concentrated flow modelling approach, the model was enhanced to be a practical tool that utilizes readily available vegetation and soil data for quantifying erosion and assessing erosion risk following rangeland disturbance. Copyright © 2014 John Wiley & Sons, Ltd.

KEY WORDS    erosion modelling; fire; woodland encroachment; rangeland management; dynamic erodibility; stream power

*Received 1 May 2013; Accepted 29 January 2014*

## INTRODUCTION

Millions of acres of US rangelands have been degraded through burning, overgrazing, and woody plant encroachment (Schlesinger *et al.*, 1990; Brown *et al.*, 2005; Miller *et al.*, 2005; Wilcox, 2010; Davies *et al.*, 2011). These disturbances alter the site ecological characteristics and hydrological behaviour that, in turn, lead to increased soil loss (Pierson *et al.*, 2001, 2007, 2008a, 2011, 2013; Williams *et al.*, 2013). Many rangeland conservation practices are aimed at reducing soil loss associated with disturbances (Briske, 2011; Spaeth *et al.*, 2013). In order to quantify the potential benefits of rangeland conservation practices, land managers need reliable tools to predict soil loss under baseline conditions and following land management actions. In recent years, research has been undertaken to develop such tools. One of these new tools is the rangeland hydrology and erosion model (RHEM) (Nearing *et al.*, 2011).

The rangeland hydrology and erosion model was developed for assessing the run-off, soil erosion rate, and sediment delivery rate and volume for rainfall events at the hillslope scale. RHEM is a modified and improved version of the Water Erosion Prediction Project (WEPP) model (Flanagan and Nearing, 1995). The model was initially developed for functionally intact rangelands where concentrated flow erosion is minimal and most

*Correspondence to: Osama Z. Al-Hamdan, USDA, Agricultural Research Service, Northwest Watershed Research Center, Boise, ID, USA.
E-mail: osama.al-hamdan@ars.usda.gov

soil loss occurs by rain splash and sheet erosion processes. RHEM includes a new splash and sheet equation that was developed by Wei *et al.* (2009) using rainfall simulation data from rangelands and has parameterization equations for functionally intact rangelands. The original version of RHEM adapted WEPP's cropland-based shear stress approach for modelling concentrated flow erosion.

Recent studies show that concentrated flow is the dominant erosion process on disturbed rangelands (Pierson *et al.*, 2008a, 2009, 2010, 2013; Al-Hamdan *et al.*, 2013; Williams *et al.*, 2013). Connected patches of bare ground on disturbed rangelands promote formation of well-organized concentrated flow paths that rapidly accelerate run-off velocity and the ability of water to erode and transport sediment downslope (Wilcox *et al.*, 1996; Pierson *et al.*, 2008a, 2009; Urgeghe *et al.*, 2010; Pierson *et al.*, 2013; Williams *et al.*, 2013). The hydraulics of concentrated flow on disturbed rangelands is largely controlled by discharge, the amount of ground cover, and hillslope angle (Al-Hamdan *et al.*, 2012a, 2013). Concentrated flow on disturbed rangelands typically exhibits a dynamic erodibility, where erodibility is high at the beginning of a run-off event and then declines exponentially mainly because of reduction of availability of disturbance-source sediment (Al-Hamdan *et al.*, 2012b). Also, Al-Hamdan *et al.* (2012b) showed that stream power provides the best linear relationship among five hydraulic parameters that were tested to describe concentrated flow detachment rate for burned and tree-encroached rangelands.

The unique characteristics of concentrated flow hydraulics and erodibility on disturbed rangelands imply that a rangeland-based concentrated flow erosion modelling approach is needed. The goal of this study is to enhance the application of RHEM on a disturbed rangeland using a new approach for predicting concentrated flow erosion based on the work of Al-Hamdan *et al.* (2012a,b, 2013). For this paper, we defined disturbance as any change that results in loss of understory plants and ground cover, increases bare soil, and increases connectedness of concentrated flow paths that promote accelerated soil erosion and sediment yield (Davenport *et al.*, 1998; Miller *et al.*, 2005; Petersen *et al.*, 2009; Pierson *et al.*, 2010, 2013; Williams *et al.*, 2013). We present burning and the process whereby western juniper trees have encroached into sagebrush plant communities as examples of such disturbance. The specific objectives of this paper are the following: (1) present new model formulations for predicting concentrated flow erosion based on stream power and dynamic or constant erodibility approaches and (2) evaluate enhanced model performance across varying degrees of landscape disturbance.
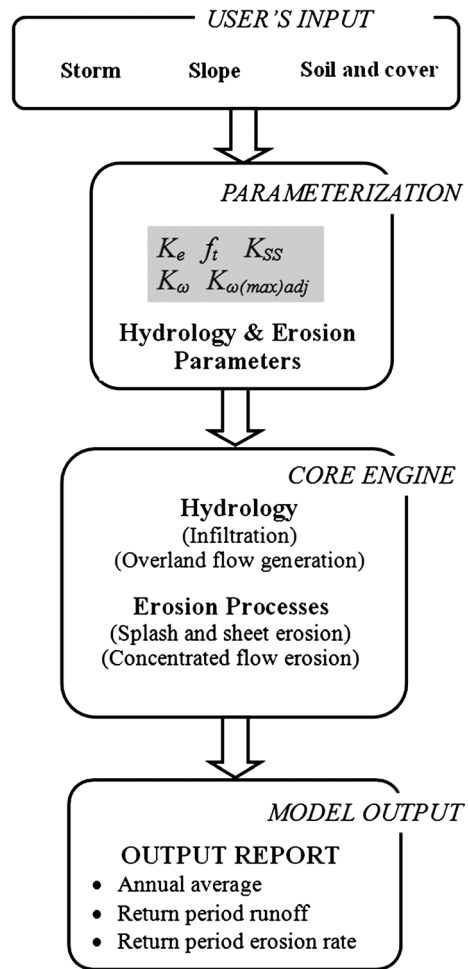


Figure 1. A flow chart of RHEM erosion prediction procedure

## METHODOLOGY

### Model description

The rangeland hydrology and erosion model simulates hillslope run-off and erosional responses based on two process model components within the core engine, hydrology and erosion (Figure 1). The hydrology component of the enhanced RHEM model is based on the KINEROS2 (K2) model (Smith *et al.* 1995). The conceptual model of soil hydrology in K2 represents a soil of either one or two layers, with the upper layer of arbitrary depth. Infiltration may occur from either rainfall directly on the soil or from ponded surface water created from upslope rainfall excess (Figure 2). At the beginning of a storm and prior to ponding, the infiltration rate is rain limited and equal to the rate of precipitation. If the rainfall intensity is greater than the saturated hydraulic conductivity, then at the onset of run-off, the infiltration rate approaches the infiltration capacity that is described by the Parlange three-parameter model (Parlange *et al.* 1982):
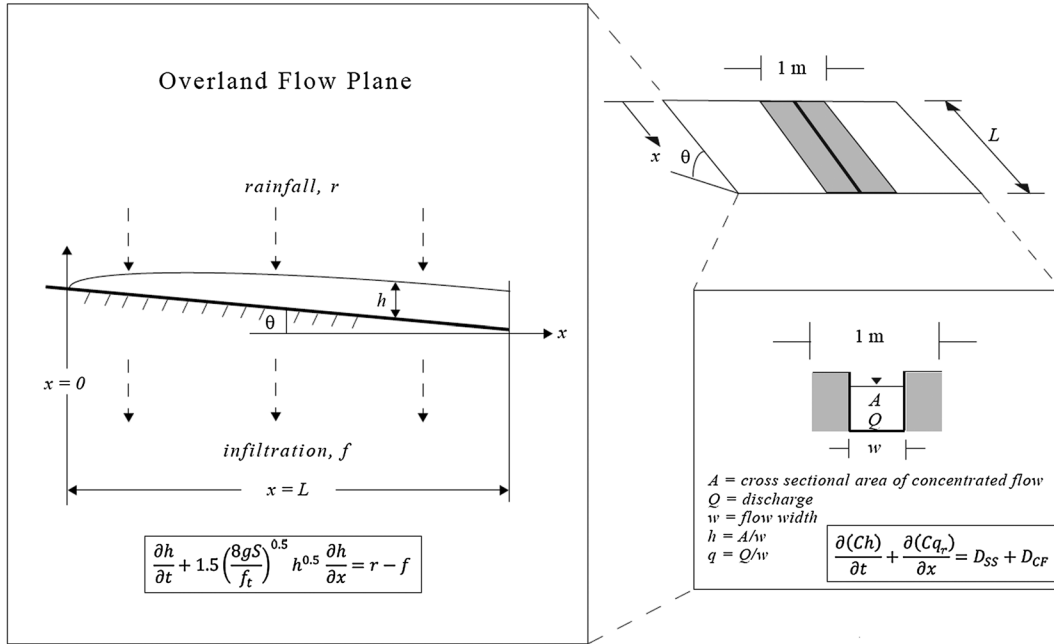
Figure 2. A diagram of the overland flow and erosion routing procedure in enhanced RHEM

$$f = K_e \left[ 1 + \frac{\alpha}{\exp\left(\frac{\alpha I}{(G+h)(\theta_s - \theta_i)}\right) - 1} \right] \qquad (1)$$

where $f$ is the infiltration capacity (m s$^{-1}$), $I$ is the cumulative depth of the water infiltrated into the soil (m), $\theta_s$ is the soil porosity (m$^3$ m$^{-3}$), $\theta_i$ is the initial (antecedent) soil moisture content, $\alpha$ is a parameter between 0 and 1, $h$ is the depth of surface flow, and $K_e$ is the soil effective saturated hydraulic conductivity (m s$^{-1}$). When $\alpha = 0$, Equation (1) is reduced to the familiar Green and Ampt infiltration model (Green and Ampt, 1911), and when $\alpha = 1$, the equation simplifies to the Smith and Parlange (1978) model. In this study, $\alpha$ was set at a value near to zero (i.e. 0.03) in order to reduce Equation (1) to an approximation of the Green–Ampt infiltration model. The effective net capillary drive ($G$) is the integrated capillary head across the wetting front (Smith *et al.*, 1993):

$$G(\psi_i) = \int_0^{\psi_i} \left( \frac{K(\psi)}{K_e} \right) d\psi \qquad (2)$$

in which $\psi$ is the soil water capillary head taken as positive (m), $\psi_i$ is the initial (antecedent) soil capillary head (m), and $K$ is hydraulic conductivity (m s$^{-1}$). The parameter $G$ (m) accounts for the effect of capillary forces on moisture absorption during infiltration.

The solution of the following equation is used to rout the rainfall excess:

$$\frac{\partial h}{\partial t} + \frac{\partial q}{\partial x} = v \qquad (3)$$

where $h$ is the depth of flow (m), $q$ is discharge per unit width (m$^2$ s$^{-1}$), and $v$ is the rainfall excess (m s$^{-1}$) that is calculated by the following equation:

$$v = r - f \qquad (4)$$

where $r$ is the rainfall rate (m s$^{-1}$), and $f$ is the infiltration rate (m s$^{-1}$).

The relationship between $q$ and $h$ is represented by the following equation:

$$q = \left( \frac{8gS}{f_t} \right)^{0.5} h^{1.5} \qquad (5)$$

where $g$ is the gravity acceleration (m s$^{-2}$), $S$ is the slope (m m$^{-1}$), and $f_t$ is the Darcy–Weisbach friction factor estimated by (Al-Hamdan *et al.*, 2013)

$$\log(f_t) = -0.109 + 1.425 res + 0.442 rock \\ + 1.764 bascry + 2.068 S \qquad (6)$$

where $res$ is the fraction of area covered by litter to total area (m$^2$ m$^{-2}$), *bascry* is the fraction of area covered by basal plants and cryptogams to total area (m$^2$ m$^{-2}$), and *rock* is the fraction of area covered by rock to total area (m$^2$ m$^{-2}$). Substituting Equations (4) and (5) in Equation (3) results in the hydrology routing equation:

$$\frac{\partial h}{\partial t} + 1.5\left(\frac{8gS}{f_t}\right)^{0.5} h^{0.5} \frac{\partial h}{\partial x} = r - f \qquad (7)$$

The erosion component in enhanced RHEM calculates sediment rate as the total detachment rate of concentrated flow and rain splash and sheet flow using a dynamic partial differential sediment continuity equation:

$$\frac{\partial (Ch)}{\partial t} + \frac{\partial (Cq_r)}{\partial x} = D_{SS} + D_{CF} \qquad (8)$$

where $C$ is the measured sediment concentration (kg m$^{-3}$), $q_r$ is the flow discharge of concentrated flow per unit width (m$^2$ s$^{-1}$), $D_{SS}$ is the splash and sheet detachment rate (kg s$^{-1}$ m$^{-2}$), and $D_{CF}$ is the concentrated flow detachment rate (kg s$^{-1}$ m$^{-2}$).

For a 1-m wide plane, when overland flow accumulates into a concentrated flow path, the concentrated flow discharge per unit width ($q_r$) is calculated by the following equation:

$$q_r = \frac{q}{w} \qquad (9)$$

where $w$ is the concentrated flow width (m) calculated by (Al-Hamdan *et al.*, 2012a)

$$w = \frac{2.46 Q^{0.39}}{S^{0.4}} \qquad (10)$$

The splash and sheet detachment rate ($D_{SS}$) is calculated as in the original version of RHEM by the following equation (Wei *et al.*, 2009):

$$D_{SS} = K_{SS} r^{1.052} q^{0.592} \qquad (11)$$

where $K_{SS}$ is the splash and sheet erodibility, and $r$ is the rainfall intensity (m s$^{-1}$).

Concentrated flow detachment rate ($D_{CF}$) is calculated as the net detachment and deposition rate (Foster, 1982):

$$D_{CF} = \begin{bmatrix} D_C\left(1 - \frac{CQ}{T_c}\right), CQ \leq T_c \\ \frac{0.5 V_f}{Q}(T_c - CQ), CQ \geq T_c \end{bmatrix} \qquad (12)$$

where $D_C$ is the concentrated flow detachment capacity (kg s$^{-1}$ m$^{-2}$), $Q$ is the flow discharge (m$^3$ s$^{-1}$), $T_c$ is the sediment transport capacity (kg s$^{-1}$), and $V_f$ is the soil particle fall velocity (m s$^{-1}$) that is calculated as a function of particle density and size (Fair *et al.*, 1971). Soil particle fall velocity is calculated using the mean particle size ($D_{50}$) of the soil texture.

Sediment detachment rate from concentrated flow is calculated using soil erodibility of the site and hydraulic parameters of the flow such as flow width and stream power. Soil detachment is assumed to start when concentrated flow starts (i.e. no threshold concept for initiating detachment is used) (Al-Hamdan *et al.*, 2012b).

In the case where dynamic erodibility concept is used, concentrated flow erodibility is set to be high at the beginning of the event and then decreases exponentially because of the reduction of the availability of disturbance-source sediment (Al-Hamdan *et al.*, 2012b):

$$D_C = K_{\omega(Max)adj} \exp(\beta q_c)\omega \qquad (13)$$

$$q_c = \int q_r dt \qquad (14)$$

$$\omega = \gamma S q_r \qquad (15)$$

where $K_{\omega(max)adj}$ is the maximum stream power erodibility (s$^2$ m$^{-2}$) corresponding to the decay factor ($\beta = -5.53$ m$^{-2}$), $\beta$ is a decay coefficient representing erodibility change during an event (m$^{-2}$), $\omega$ is the stream power (kg s$^{-3}$), $q_c$ is the cumulative flow discharge of concentrated flow per width unit (m$^2$), $\gamma$ is the water specific weight (kg m$^{-2}$ s$^{-2}$), and $S$ is the slope (m m$^{-1}$).

To calculate $D_C$ for the case of constant erodibility, where $\beta = 0$, Equation (13) becomes (Al-Hamdan *et al.*, 2012b)

$$D_C = K_\omega(\omega) \qquad (16)$$

where $K_\omega$ is the event-constant stream power erodibility factor (s$^2$ m$^{-2}$). To calculate the transport capacity ($T_c$), the empirical equation of Nearing *et al.* (1997) is used:

$$Log_{10}\left(\frac{10 T_c}{w}\right) = -34.47 + 38.61$$
$$* \frac{\exp[0.845 + 0.412 \log(1000\omega)]}{1 + \exp[0.845 + 0.412 \log(1000\omega)]} \qquad (17)$$

*Study sites and experimental data*

The data used for evaluating the model were obtained from published rainfall simulation experiments conducted on three disturbed rangeland sites. The first site, Breaks, is located in the USDA, Agricultural Research Service, Reynolds Creek Experimental Watershed, Idaho. This sagebrush site was disturbed by moderate-severity to high-severity prescribed fire. Rainfall simulation experiments (60 min, 60 mm h$^{-1}$) were conducted on eight plots (6.5-m long by 5-m wide, large rainfall plots) before the fire and on eight burned plots immediately after fire. Rainfall simulation experiments were replicated on eight additional randomly selected burned plots 1 and 2 years after the fire. For more information about the Breaks site and experiments, refer to Moffet *et al.* (2007) and Pierson *et al.* (2009).

The second site, Steens, is located in south-eastern Oregon. This historical sagebrush site is in the later stages of woodland (western juniper) encroachment and has a degraded understory with extensive, well-connected bare ground within the intercanopy (area between trees). A part of the site was treated by cutting trees, which resulted in some degree of recovery of the intercanopy vegetation cover after 10 years. Rainfall simulation experiments (60 min, 55 mm h$^{-1}$) were conducted on 16 plots (6.5-m long by 5-m wide) in the intercanopy area (eight plots on the degraded uncut area and eight plots on the recovered area 10 years after tree cutting). For more information about the Steens site and experiments, refer to Pierson *et al*. (2007).

The third site, Castlehead, is located in south-western Idaho. This sagebrush site has been disturbed by woodland (western juniper) encroachment and by subsequent wildfire in some areas. Rainfall simulation experiments (45 min, 102 mm h$^{-1}$) were conducted on 18 plots (6.5-m long by 2-m wide) where six plots were located in the burned intercanopy area, six plots in the unburned intercanopy area, and six plots in the burned tree zone (area directly underneath tree canopy pre-fire). For more information about the Castlehead site and experiments, refer to Pierson *et al*. (2013) and Williams *et al*. (2013).

Slope and ground cover as well as sediment rates and run-off were measured for each plot at the three sites. Splash and sheet erosion estimates were obtained from small rainfall simulation plots (0.7-m long by 0.7-m wide) in which concentrated flow does not form (Pierson *et al*. 2009, 2013; Williams *et al*. 2013). These values then were upscaled to the large plots (Williams *et al*., 2013) to determine the fraction of splash and sheet erosion to total erosion value. Splash and sheet estimates were only available for burned plots 1- and 2-year post-fire at

Breaks and 1-year post-fire at Castlehead. Small plot rainfall simulations were not conducted at the Steens site (Pierson *et al*., 2007). Only data from plots that generated run-off were used for the model evaluation analysis. For the Breaks and Castlehead sites, only data from plots where site-specific calibrated concentrated flow erodibility was available were used for the model evaluation analysis. Table I shows a summary of the site characteristics and experiments that were used for evaluating the new concentrated flow erosion modelling approach.

*Model parameterization*

To test the performance of the new stream-power-based concentrated flow erosion modelling approach for cases of constant (average value within the run-off event) and dynamic erodibility, $K_e$ and initial saturation were optimized on the total volume of run-off and run-off starting time, respectively. By using optimized $K_e$ values, average total run-off converged within less than 0.01 mm of the average of the measured values for all plots. Time for run-off was within a minute of actual start time for run-off in each plot. The erosion model performance was analysed in different parameterization schemes for erodibility.

In the first parameterization scheme, the model performance was tested using erodibility parameters estimated by empirical equations developed from rangeland experimental sites (Al-Hamdan *et al*. 2012b) as follows.

For the dynamic erodibility case, the maximum initial concentrated flow erodibility ($K_{\omega(max)adj}$) was estimated by

$$log_{10}\left(K_{\omega(max)adj}\right) = -3.64 - 1.97(res+bascry)$$
$$-1.85rock - 4.99clay + 6.06silt \qquad (18)$$

Table I. Experimental sites used to evaluate the new RHEM version

| Site | Treatment | Years after treatment | No. of plots | No. of plots used for evaluation | Slope | Applied rainfall (mm) | Rainfall duration (min) |
|---|---|---|---|---|---|---|---|
| Breaks | All | — | 32 | 25 | 43 | 65 | 60 |
| | Burned | 0 | 8 | 8 | 42 | 59 | 60 |
| | Burned | 1 | 8 | 6 | 42 | 70 | 60 |
| | Burned | 2 | 8 | 7 | 45 | 67 | 60 |
| | Unburned | — | 8 | 4 | 40 | 65 | 60 |
| Castlehead | All | — | 18 | 15 | 18 | 85 | 45 |
| | Burned intercanopy | 1 | 6 | 4 | 16 | 85 | 45 |
| | Unburned intercanopy | — | 6 | 5 | 20 | 86 | 45 |
| | Burned trees | 1 | 6 | 6 | 18 | 84 | 45 |
| Steens | All | — | 16 | 10 | 19 | 54 | 60 |
| | Cut trees | 10 | 8 | 2 | 19 | 55 | 60 |
| | Uncut trees | — | 8 | 8 | 19 | 54 | 60 |
| All | | — | 66 | 50 | — | — | — |

In the constant erodibility case for burned plots, erodibility ($K_\omega$) was estimated by

$$log_{10}(K_\omega)=-3.29-2.25(res+bascry)-1.82rock+3.95silt \tag{19}$$

In the constant erodibility case for unburned (undisturbed or woodland encroached) plots, erodibility ($K_\omega$) was estimated by

$$log_{10}(K_\omega)=-4.14-1.28res-0.98rock-15.16clay+7.09silt \tag{20}$$

Splash and sheet erodibility ($K_{SS}$) was estimated by (Hernandez *et al.*, 2013)

$$log_{10}(K_{SS})=4.01-1.18rock-0.982(litter+cancov) \tag{21}$$

where *litter* is the fraction of area covered by litter to total area ($m^2\,m^{-2}$), and *cancov* is the fraction of area covered by canopy to total area ($m^2\,m^{-2}$).

In the second parameterization scheme, the erosion model was tested when using calibrated $K_{SS}$, while $K_{\omega(max)adj}$ and $K_\omega$ were estimated by the empirical equations (Equations (18)–(20)). The purpose of this parameterization scheme is to strictly test the performance of the concentrated flow erosion modelling approach by eliminating the error generated from the splash and sheet erosion component in the model. $K_{SS}$ was calibrated by setting concentrated flow erosion erodibility as zero while changing the $K_{SS}$ value until it converged to the measured splash and sheet erosion with an error margin of less than 1%. The errors generated from splash and sheet erosion were estimated by comparing the simulated erosion values, when using Equation (21) to estimate $K_{SS}$, against the measured splash and sheet erosion.

The model was also run using calibrated $K_{SS}$, but calibrated $K_{\omega(max)adj}$ and $K_\omega$ values were obtained from concentrated flow experiments at the Breaks site (Al-Hamdan *et al.*, 2012b).

The purpose of this parameterization scheme is to assess error generated from the concentrated flow erodibility empirical estimation equations (Equations (18)–(20)). Values of erodibility parameters used for all parameterization schemes are shown in Table II.

*Statistical analysis*

Mean value and standard error of simulated erosion with each parameterization scheme were calculated within each study-year-treatment combination to compare simulated and measured erosion. Mean value and standard error of simulated time series erosion rate using calibrated $K_\omega$ and $K_{\omega(max)adj}$ and calibrated $K_{SS}$ were calculated for the burned tree plots at the Castlehead site to compare the constant and dynamic erodibility concept performance. Coefficient of determination ($R^2$), Nash–Sutcliffe efficiency (*NSE*) (Nash and Sutcliffe, 1970), percent bias (*PBIAS*) (Gupta *et al.*, 1999), ratio of root-mean-square error to standard deviation (*RSR*) (Legates and McCabe, 1999), and relative difference error (*Rdiff*) (Nearing, 2000) were used to evaluate the overall performance of the model to predict soil erosion for all sites and treatments, when using estimated $K_{\omega(max)adj}$ and $K_\omega$ and calibrated $K_{SS}$.

$R^2$ was calculated by

$$R^2 = \left( \frac{\sum_{i=1}^{n}(O_i - O_{avg})(M_i - M_{avg})}{\sqrt{\sum_{i=1}^{n}(O_i - O_{avg})^2}\sqrt{\sum_{i=1}^{n}(M_i - M_{avg})^2}} \right)^2 \tag{22}$$

*NSE* was calculated by

$$NSE = 1 - \frac{\sum_{i=1}^{n}(O_i - M_i)^2}{\sum_{i=1}^{n}(O_i - O_{avg})^2} \tag{23}$$

Table II. Average values of estimated and site-specific calibrated concentrated flow erodibility parameters ($K_\omega$ and $K_{\omega(max)adj}$) and estimated and calibrated splash and sheet erodibility ($K_{SS}$) for burned plots at the Breaks and Castlehead sites and tree-encroached plots at the Steens site used for running the model

| Site | Disturbance | Years after fire | $K_\omega$ ($10^{-3}\,s^2\,m^{-2}$) | | $K_{\omega(max)adj}$ ($10^{-3}\,s^2\,m^{-2}$) | | $K_{SS}$ ($10^3$) | |
|------|-------------|------------------|-----------|------------|-----------|------------|-----------|------------|
| | | | Estimated | Calibrated | Estimated | Calibrated | Estimated | Calibrated |
| Breaks | Burned | 0 | 1.42 | 2.1 | 1.64 | 2.9 | 5.91 | 23.44 |
| | Burned | 1 | 0.94 | 2.56 | 1.15 | 3.81 | 1.8 | 89.09 |
| | Burned | 2 | 0.19 | 0.89 | 0.28 | 1.59 | 0.44 | |
| Castlehead | Burned intercanopy | 1 | 1.39 | 1.09 | 2.15 | 2.03 | 1.0 | 2.04 |
| | Burned tree | 1 | 2.19 | 3.04 | 5.35 | 5.39 | 2.51 | 2.33 |
| Steens | Tree encroached | | 0.19 | — | 4.91 | — | 6.27 | — |

*PBIAS* was calculated by

$$PBIAS = \frac{\sum_{i=1}^{n}(O_i - M_i)*100}{\sum_{i=1}^{n}(O_i)} \quad (24)$$

*RSR* was calculated by

$$RSR = \frac{\sqrt{\sum_{i=1}^{n}(O_i - M_i)^2}}{\sqrt{\sum_{i=1}^{n}(O_i - O_{avg})^2}} \quad (25)$$

and *Rdiff* was calculated by

$$Rdiff = \frac{(M_i - O_i)}{(M_i + O_i)} \quad (26)$$

where $O_i$ is the $i$th observation to be evaluated, $M_i$ is the simulated value by the model for the corresponding $i$th observation, $O_{avg}$ is the average of the observed values, $M_{avg}$ is the average of simulated values, and $n$ is the number of observations. *Rdiff* was compared with 95% confidence interval of relative difference error because of natural variability between plots calculated by Nearing (2000) from a large number of replicated plot data.

## RESULTS AND DISCUSSION

### Model performance with estimated $K_{SS}$

The performance of the enhanced RHEM model when $K_{SS}$ was estimated using empirical Equation (21) varied among sites and disturbance types. For the Breaks site, using estimated $K_\omega$ and $K_{\omega(max)adj}$ for the constant and dynamic erodibility concepts poorly predicted soil erosion with respect to measured values of the first few years after post-fire (Figure 3). Both concepts predicted

~40% of the measured erosion immediately following fire and predicted 20–25% of the measured erosion 1-year post-fire (Figure 3a). The estimated erodibility model using the dynamic concept predicted ~50% and more than 80% of the measured erosion for the second year post-fire and unburned conditions, respectively (Figure 3b). However, measured concentrated flow erosion rates were low on burned plots by the second year following fire and on unburned plots. There was no major difference between the soil erosion predicted in the unburned plots using the constant *versus* dynamic erodibility concepts. A large part of the total erosion underestimation in the first few years post-fire at Breaks can be explained by the error in splash and sheet erosion estimates. As can be seen in Figure 4a, using estimated $K_{SS}$, the model predicted only 26% of the measured splash and sheet erosion (4.6 ton ha$^{-1}$) for burned plots immediately after fire. In the burned plots 1 year after fire, the model predicted 37% of the measured splash and sheet erosion (0.54 ton ha$^{-1}$). Percentage of simulated splash and sheet erosion to total erosion in the unburned plots at the Breaks was relatively high (44%).

At the Steens site, the constant and dynamic erodibility concepts similarly predicted the measured effects of tree cutting on soil erosion, but the dynamic erodibility concept greatly overpredicted soil erosion from the uncut plots (Figure 5). Measured soil erosion was generally low (0.06 ton ha$^{-1}$) in the cut woodland and was only slightly less than that predicted by the constant and dynamic concepts. For uncut plots, measured and constant erodibility-predicted soil erosion were both slightly greater than 1 ton ha$^{-1}$, whereas the dynamic concept (Equation (13)) predicted nearly 3 ton ha$^{-1}$ of soil erosion. We attribute the significantly greater soil loss predicted by the dynamic erodibility to the fact that the dynamic erodibility estimation equation (Equation (18)) was derived from data collected on burned rangelands with ample detachable sediment supply (Al-Hamdan *et al.* 2012b). Simulated splash and sheet erosion at the Steens provided the majority of total simulated erosion (84% in the uncut plots and 98% in the cut plots). Even though
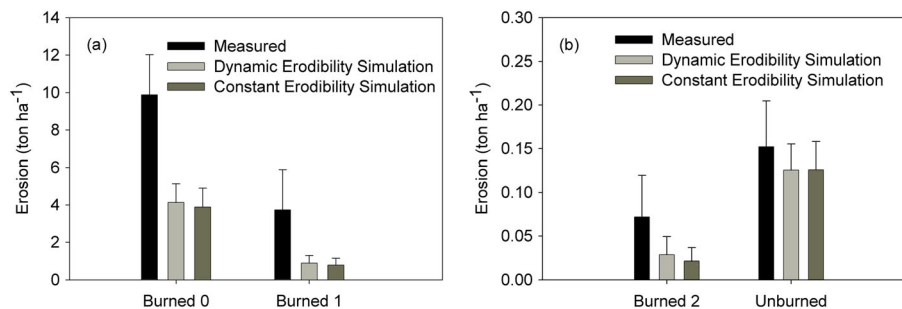


Figure 3. Measured and simulated erosion using dynamic and constant erodibility approaches with estimated concentrated flow and splash and sheet erodibility parameters at the breaks site: (a) immediately after fire (burned 0) and 1 year after fire (burned 1); (b) 2 years after fire (burned 2) and unburned. Error bars represent standard error
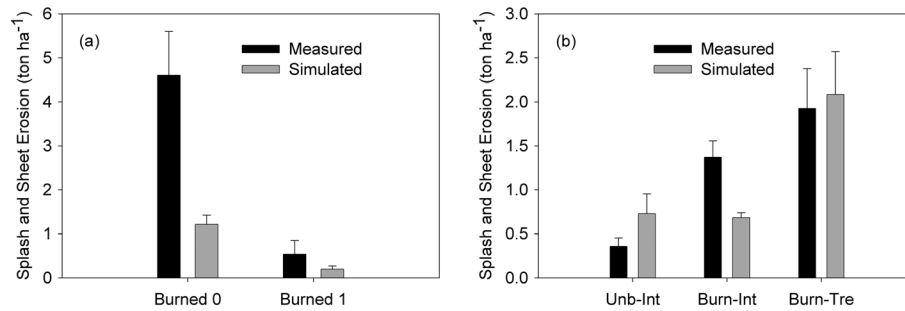
Figure 4. Measured and simulated splash and sheet erosion with estimated splash and sheet erodibility parameters at the following: (a) the breaks site, immediately after fire (burned 0) and 1 year after fire (burned 1); (b) the Castlehead site, unburned intercanopy (Unb-Int), burned intercanopy (Burn-Int), and burned trees (Burn-Tre). Error bars represent standard error
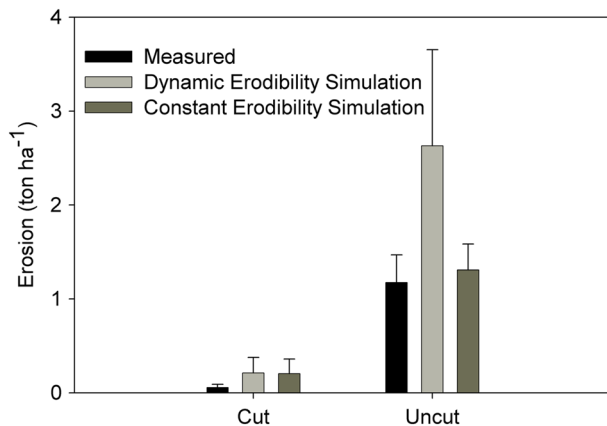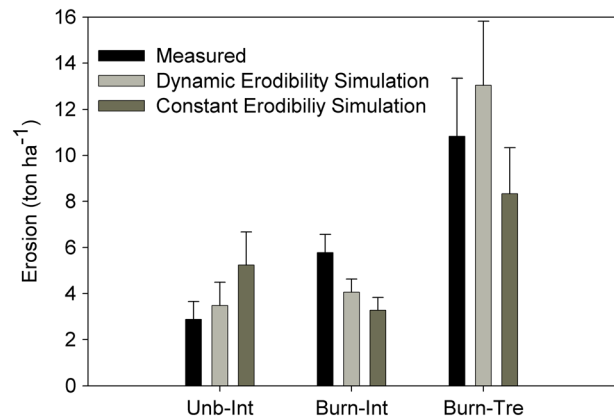


Figure 5. Measured and simulated erosion using dynamic and constant erodibility approaches with estimated concentrated flow and splash and sheet erodibility parameters at the steens site. Error bars represent standard error



Figure 6. Measured and simulated erosion using dynamic and constant erodibility approaches with estimated concentrated flow and splash and sheet erodibility parameters at the Castlehead site, unburned intercanopy (Unb-Int), burned intercanopy (Burn-Int), and burned trees (Burn-Tre). Error bars represent standard error

measured splash and sheet erosion was not available for comparison in these plots, model prediction of splash and sheet being the major source of erosion was consistent with the field observations at these plots where incised concentrated flow paths were absent (Pierson *et al.* 2007).

At the Castlehead site, applying the constant erodibility concept when using estimated values of erodibility, simulated erosion (5.24 ton ha$^{-1}$) was twofold larger than measured erosion (2.88 ton ha$^{-1}$) in the unburned intercanopy (Figure 6). Using the dynamic erodibility, the error was reduced to 21%, where simulated erosion was 3.48 ton ha$^{-1}$. In burned intercanopy, the constant erodibility concept predicted 57% and the dynamic erodibility concept predicted 70% of the measured erosion. In the burned tree area at Castlehead, the constant erodibility underestimated measured erosion by 23%, while the dynamic approach overestimated the actual values by 21%. Error in simulating overall splash and sheet erosion at the Castlehead site varied depending on plot locations (Figure 4b). The model overestimated the measured splash and sheet erosion by twofold (0.4 ton ha$^{-1}$) in the unburned intercanopy, and it

predicted only half of the measured (1.4 ton ha$^{-1}$) splash and sheet erosion in the burned intercanopy. The error in estimating splash and sheet erosion was only 8% in the burned tree plots.

Fire at the Breaks and Castlehead sites not only increased concentrated flow erosion but it also increased splash and sheet erosion. The estimation equation for $K_{SS}$ (Equation (21)) reasonably detected the overall increase of erosion from burned tree plots at Castlehead but not from burned plots at Breaks (Figure 4). Slope averages at Breaks and Castlehead plots were 43% and 18%, respectively. The slope difference suggests that even though Equation (21) was developed from undisturbed rangeland, it can be used to estimate $K_{SS}$ for gently sloped disturbed rangeland. However, the combined conditions of fire and steep slope angle may require a different estimation equation. For steeply sloped burned conditions, gravitational effects on detachment resistance become minor relative to those on gentle terrain (Moody *et al.*, 2005), and the relationship between erosion rate and energy of rainfall and sheet flow is enhanced. The use of stream-power-based transport capacity allows the

model to address the increase in concentrated flow erosion for highly disturbed sites similar to the burned plots at Breaks. However, a new modelling approach for splash and sheet erosion or new parameterization approach for $K_{SS}$ might be needed for such conditions to address the slope effect on the relationship between erosion rate and energy of rainfall and sheet flow.

*Model performance with calibrated $K_{SS}$*

In order to assess the performance of, strictly, the concentrated flow erosion modelling approaches, we eliminated the error associated with splash and sheet erosion through calibrating $K_{SS}$. In general, replacing estimated $K_{SS}$ by a calibrated value reduced the overall error in predicting total erosion. Both dynamic and constant erodibility predicted most of the total measured erosion (70–74%) from burned plots immediately after fire at the Breaks (Figure 7a). Calibrating $K_{SS}$ improved prediction of total erosion in the burned plots at Breaks 1 year after fire when using the dynamic erodibility concept. However, simulated erosion was still low with respect to the measured erosion (33%). Removing the splash and sheet erosion error reduced the overall erosion prediction error in the unburned intercanopy plots at Castlehead from 21 to 9% when using the dynamic erodibility (Figure 7b). Error in total erosion prediction reduced from 82 to 70% when using constant erodibility. Calibrating $K_{SS}$ also reduced the simulated error in the burned intercanopy plots at Castlehead to less than 20% when using the dynamic erodibility concept and 31% when using the constant erodibility. For burned tree plots, calibrating $K_{SS}$ slightly reduced error to 19% in the dynamic erodibility case, whereas it increased the error slightly in the constant erodibility case to 25%.

The error in total erosion prediction after eliminating the splash and sheet error can be explained by two major sources. The first error comes from the uncertainty of a concentrated flow erodibility estimation equation. For instance, reducing this source of error by using the calibrated erodibility $K_{\omega(max)adj}$ for the burned plots at Breaks ( 1 year after fire) increased the simulated erosion values to 3.05 ton ha$^{-1}$ (82% of the measured value) (Figure 8). Calibrated $K_{\omega}$ also increased the estimated erosion for these plots to 2.24 ton ha$^{-1}$ (60% of the measured erosion) with respect to using estimated $K_{\omega}$ (Figure 8). Given the fact that measured erosion (erodibility) has natural spatial variability within the same site (Wendt *et al.*, 1986; Nearing, 2000), the error generated from the estimation equations is still reasonable. This natural variability is reduced in the case of high erosion (Wendt *et al.*, 1986; Nearing, 2000) such as in the burned plots immediately after a year, where the error generated from the erodibility estimation equations is reduced (Figure 8).

The second major source of error could be in the hydrology component. Because soil erosion is highly dependent on run-off (Pierson *et al.*, 2010, 2013; Williams *et al.*, 2013), less accuracy in predicting run-off facilitates less accuracy in erosion prediction. Even though the model was optimized for total run-off and
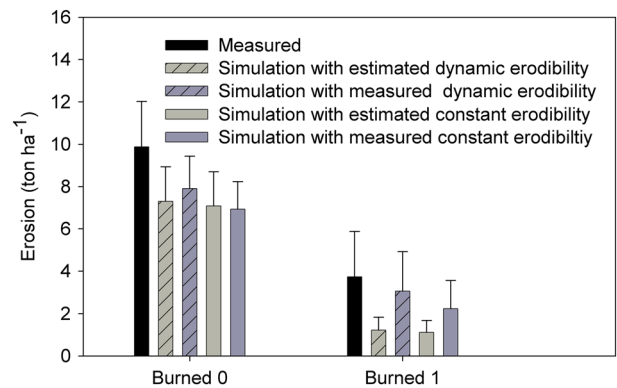


Figure 8. Measured and simulated erosion using dynamic and constant erodibility approaches with estimated and measured concentrated flow erodibility and calibrated splash and sheet erosion at the breaks site, immediately after fire (burned 0) and 1 year after fire (burned 1). Error bars represent standard error
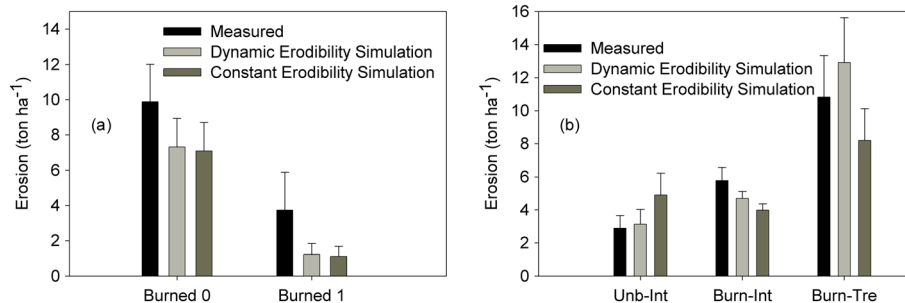


Figure 7. Measured and simulated erosion using dynamic and constant erodibility approaches with estimated concentrated flow erodibility and calibrated splash and sheet erosion for the high erodible plots at the following: (a) the breaks site, immediately after fire (burned 0) and 1 year after fire (burned 1); (b) the Castlehead site, unburned intercanopy (Unb-Int), burned intercanopy (Burn-Int), and burned trees (Burn-Tre). Error bars represent standard error

run-off starting time, the shape of the hydrograph (e.g. peak time, rising limb, and recession limb) in some cases, such as the burned plots at Breaks (immediately after fire), was poorly simulated (Figure 9a). Water repellency in such burned sites causes the infiltration not to follow those rates indicated by the Green–Ampt model. In this situation, infiltration decreases during early stages and then increases with time, after the water repellent layer breaks down, until it (if sufficient time passes) reaches steady state infiltration (Meeuwig 1971; Imeson *et al.*, 1992; Robichaud, 2000; Pierson *et al.*, 2001, 2008b, 2010). Soil water repellency on burned tree plots at Castlehead also reduced the infiltration rate. The low infiltration resulted in an early start of run-off as well as high total run-off. However, the impact of the water repellent layer on hydrograph shape was not apparent (Figure 9b). Soil water repellency was strong to a depth of 5 cm at Castlehead (Williams *et al.*, 2013), thus wetting up of the thick repellent layer may not have occurred during the rainfall simulation.

### Recommended applications in RHEM

Based on the results in the preceding texts, we recommend using the dynamic erodibility concept for sites with relatively immediate disturbance, such as fire,

for modelling concentrated flow erosion in RHEM. Using dynamic erodibility instead of constant erodibility improved the model performance on these sites by addressing the instantaneously elevated sediment pulse generated by the disturbance. The differences in the performance of the constant erodibility *versus* dynamic concepts can be more important in smaller rainfall events. Using constant erodibility would have reasonable results for long run-off events like those in our rainfall simulations given that overestimation of erosion in late stages compensates for underestimation in the early stages of the run-off event. For instance, in the burned tree plots at the Castlehead site, the erosion rate simulation using constant erodibility had greater error in the first 15 min of the 45-min run (Figure 10a). The error was reduced when using the dynamic erodibility concept (Figure 10b). The return interval of a storm similar to the applied rainfall simulation (102 mm h$^{-1}$, 45 min) exceeds 100 years for the Castlehead site, while the return interval of such intensity over 10 and 15 min is 33 and 75 years, respectively (Hanson and Pierson, 2001). Therefore, using a dynamic erodibility for sites similar to the burned tree plots at Castlehead likely provides a better estimate of post-fire erosion from commonly occurring storms. The difference in the results between constant and dynamic
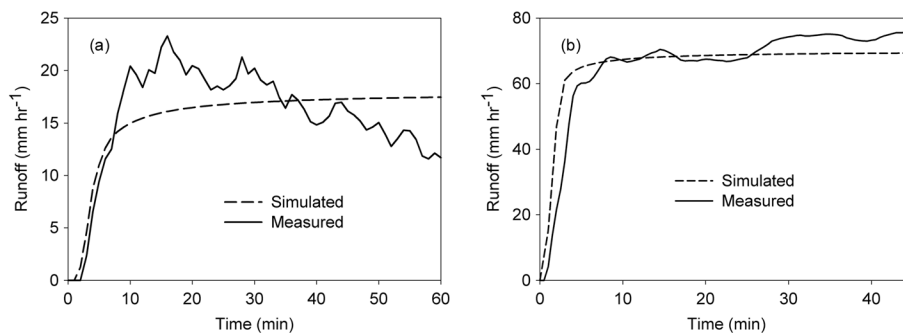


Figure 9. Measured and simulated run-off with optimizing $K_e$ and $K_{ss}$ for (a) burned plots at the breaks site immediately after fire and (b) burned tree plots at the Castlehead site
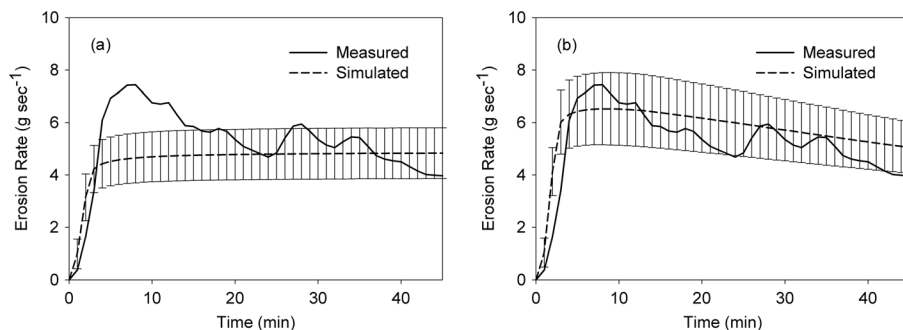


Figure 10. Measured and simulated erosion rate using (a) constant erodibility approach and (b) dynamic erodibility approach with measured concentrated flow erodibility and calibrated splash and sheet erosion for the burned tree plots at the Castlehead site. Error bars represent standard error

erodibility concepts brings the necessity of defining the timing of the measurement and estimation of average constant erodibility values. Different measurement timing with respect to run-off would result in different constant erodibility and thus different erosion estimation. The impact of this problem is reduced in the dynamic erodibility concept because only the erodibility at the beginning of each run-off event is needed.

For the undisturbed or gradually disturbed sites (e.g. woodland encroached), we recommend using the constant erodibility concept for modelling concentrated flow erosion in RHEM. For the undisturbed sites, the major source of erosion is from splash and sheet processes, and the likelihood of concentrated flow generation is small (Al-Hamdan *et al.*, 2013). For tree-encroached sites, the chance for formation of concentrated flow is higher than for undisturbed sites; however, these sites have less available sediment with respect to a newly burned site, as they have been eroding at reasonable high rates for years. This gradual reduction in sediment availability in the intercanopy reduced the significance of an immediate pulse of sediments at the beginning of a rainfall event with respect to a newly burned site. Therefore, choosing between the two concepts for modelling concentrated flow is not crucial in both undisturbed sagebrush and tree-encroached sites. Because the estimation equation for the dynamic erodibility was developed from burned sites, using constant erodibility would be recommended for the unburned sites.

The model with constant erodibility in the unburned sites and dynamic erodibility in the burned site was able to match the predicted effect of disturbances and treatments. For instance, following the measured erosion trend, simulated erosion increased dramatically immediately after fire at the Breaks and then started to decrease with years passing (Figure 8). Also, the model predicted the effect of the tree cut treatment where simulated erosion decreased significantly 10 years after cutting trees (Figure 5). The overall performance of the enhanced model using estimated $K_\omega$ and $K_{\omega(max)adj}$ had a coefficient of determination ($R^2$) of 0.78 and *NSE* of 0.71 (Figure 11). A low *RSR* and a low absolute *PBIAS* are indications for the favourable performance of the model (Moriasi *et al.*, 2007). All predictions had an *Rdiff* within the 95% occurrence of such error from a large number of replicated plot data (Figure 12), which suggests that the error in all predictions was acceptable relative to natural or expected plot-to-plot variations at a site (Nearing, 2000).

The newly presented concentrated flow erosion modelling approach has several advantages. The linear stream-power-based equation to predict detachment capacity was found to be the best predictor for soil erosion on sites with high disturbance (Al-Hamdan *et al.*, 2012b). The linearity of stream power *versus* detachment capacity allows the
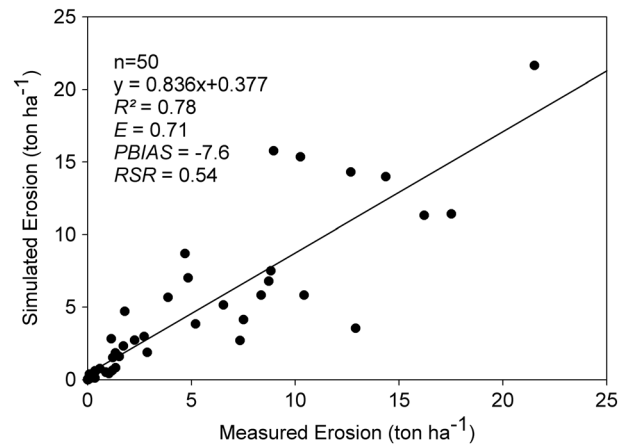


Figure 11. Measured and simulated erosion rate for all sites using constant erodibility approach at the unburned sites and dynamic erodibility approach at the burned sites with estimated concentrated flow erodibility and calibrated splash and sheet erosion
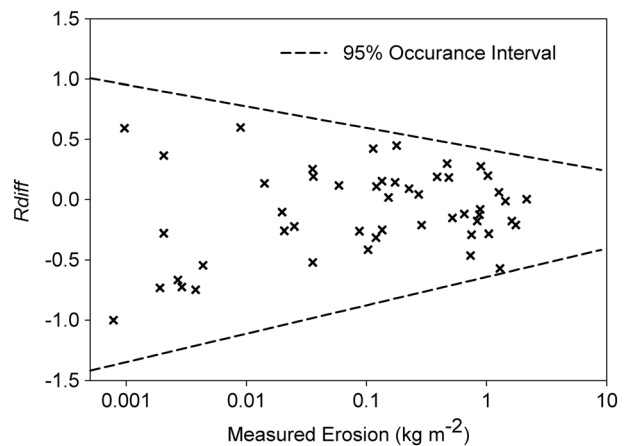


Figure 12. Relative difference between simulated and measured erosion (*Rdiff*) with measured erosion (kg m$^{-2}$) for all sites using constant erodibility approach at the unburned sites and dynamic erodibility approach at the burned sites with estimated concentrated flow erodibility and calibrated splash and sheet erosion. Dash line is the 95% interval of occurrence of Rdiff from a large number of replicated plot data (after Nearing, 2000)

concentrated flow erosion component to couple with other components in RHEM. The approach does not require a threshold value for initiating erosion that reduces the parameters needed to run the model. In addition, the results of this study show that the established estimating equations for the required concentrated erodibility parameters worked reasonably well on the tested sites. These equations were obtained from data that represent a diverse set of rangeland environments with high variability of hydraulic regime (Al-Hamdan *et al.*, 2012b). Such high variability within the data set should allow application of the enhanced RHEM model for disturbed conditions across a wide span of flow regimes, ecological sites, soils, slopes, and vegetation and ground cover conditions.

## CONCLUSIONS AND IMPLICATIONS

In this study, we enhanced the applications of the RHEM model on disturbed rangelands where concentrated flow plays a major role in the soil erosion process by incorporating a new concentrated flow erosion modelling approach. The new approach uses stream power as a driving force for detaching and transporting sediments and addresses the increase in concentrated flow erodibility because of the elevation of exposed bare soils caused by disturbance such as fire or tree encroachment. The approach addresses the instantaneously elevated sediment pulse of limited supply caused by fire by using a dynamic erodibility concept where concentrated flow erosion starts at high rates and then decreases because of the decline of sediment supply. Evaluation of the enhanced version of RHEM, including associated parameter estimation equations using plot scale experimental data at three different sites, indicated the ability of the model to predict erosion at the plot scale with a satisfactory range of error ($n = 50$, $R^2 = 0.78$, and $NSE = 0.71$). The new version of the model was able to match the predicted effect of disturbances and treatments across a wide range of ecological sites and vegetation and ground cover conditions.

Including a new concentrated flow erosion modelling approach into RHEM creates a practical management tool for quantifying erosion and assessing erosion risk following rangeland disturbance. The enhanced RHEM model is easily parameterized using readily available vegetation, soils, and ground cover data. The tool can use vegetation and ground cover data to determine the degree of disturbance, impact on erosion, and track the rate of site recovery. The enhancements to RHEM expand its applicability as a practical land management tool for conservation planning and quantifying environmental benefits of alternative conservation practices. For future work, further evaluation of the new modelling approach performance at different scales, on other sites, or other kind of disturbance would help to expand its applicability scope.

### REFERENCES

Al-Hamdan OZ, Pierson Jr. FB, Nearing MA, Stone JJ, Williams CJ, Moffet CA, Kormos PR, Boll J, Weltz MA. 2012a. Characteristics of concentrated flow hydraulics for rangeland ecosystems: implications for hydrologic modeling. *Earth Surface Processes Landforms* **37**: 157–168.

Al-Hamdan OZ, Pierson FB, Nearing MA, Williams CJ, Stone JJ, Kormos PR, Boll J, Weltz MA. 2012b. Concentrated flow erodibility for physically-based erosion models: temporal variability in disturbed and undisturbed rangelands. *Water Resources Research* **48**: W07504. DOI:10.1029/2011WR011464.

Al-Hamdan OZ, Pierson FB, Nearing MA, Williams CJ, Stone JJ, Kormos PR, Boll J, Weltz MA. 2013. Risk assessment of erosion from concentrated flow on rangelands using overland flow distribution and shear stress partitioning. *Transactions of the American Society of Agricultural and Biological Engineers* **56**(2): 539–548.

Briske DD (ed). 2011. *Conservation benefits of rangeland practices: assessment, recommendations, and knowledge gaps*. USDA-NRCS: Washington, DC, USA; 429.

Brown JR, Blank RR, McPherson GR, Tate KW. 2005. Rangelands and global changes. An issue paper Created by the Society of Range Management.

Davenport DW, Breshears DD, Wilcox BP, Allen CD. 1998. Viewpoint: sustainability of piñon-juniper ecosystems – a unifying perspective of soil erosion thresholds. *Journal of Range Management* **51**: 231–240.

Davies KW, Boyd CS, Beck JL, Bates JD, Svejcar TJ, Gregg MA. 2011. Saving the sagebrush sea: an ecosystem conservation plan for big sagebrush plant communities. *Biological Conservation* **144**: 2573–2584.

Fair GM, Geyer JC, Okun DA. 1971. *Water supply and wastewater disposal*. John Wiley and Sons: New York, 973.

Flanagan DC, Nearing MA (eds). 1995. USDA-Water Erosion Prediction Project (WEPP) hillslope profile and watershed model documentation. NSERL Report No. 10, National Soil Erosion Research Laboratory, USDA-Agricultural Research Service, West Lafayette, Indiana.

Foster GR. 1982. Modeling the erosion process. Chapter 8 in: Hydrologic modeling of small watersheds. In *ASAE Monograph No. 5*, Haan CT, Johnson HP, Brakensiek DL (eds). American Society of Agricultural Engineers: St. Joseph, MI.; 297–360.

Green WH, Ampt AG. 1911. Studies of soil physics, part I – the flow of air and water through soils. *Journal of Agricultural Science* **4**: 1–24.

Gupta HV, Sorooshian S, Yapo PO. 1999. Status of automatic calibration for hydrologic models: Comparison with multilevel expert calibration. *Journal of Hydrologic Engineering* **4**(2): 135–143.

Hanson CL, Pierson FB. 2001. Characteristics of extreme precipitation and associated streamflow in the Reynolds Creek Experimental Watershed, Idaho. In Proceedings of the 12th Symposium on Global Climate Change Variations, American Meteorological Society. January 14-19, 2001, Albuquerque, NM: J2.13-J2.16.

Hernandez M, Nearing MA, Stone JJ, Pierson FB, Wei H, Spaeth KE, Heilman P, Weltz MA, Goodrich DC. 2013. Application of a rangeland soil erosion model using National Resources Inventory data in southeastern Arizona. *Journal of Soil and Water Conservation* **68**(6): 512–525. DOI:10.2489/jswc.68.6.512.

Imeson AC, Verstraten JM, van Mulligen EJ, Sevink J.1992. The effects of fire and water repellency on infiltration and runoff under mediterranean type forest. *Catena* **19**(3-4): 345–361.

Legates DR, McCabe Jr GJ. 1999. Evaluating the use of "goodness of fit" measures in hydrologic and hydroclimatic model validation. *Water Resources Research* **35**(1): 233–241.

Meeuwig RO. 1971. Infiltration and water repellency in granitic soils. Ogden, UT, USA: US Department of Agriculture, Forest Service, IFRES-INT-111. 22.

Miller RF, Bates JD, Svejcar TJ, Pierson FB, Eddleman LE. 2005. Biology, ecology, and management of western juniper (Juniperus occidentalis). Technical Bulletin 152, Oregon State University, Agricultural Experiment Station, Corvalis, Oregon.

Moffet CA, Pierson FB, Robichaud PR, Spaeth KE, Hardegree SP. 2007. Modeling soil erosion on steep sagebrush rangeland before and after prescribed fire. *Catena* **71**(2): 218–228. DOI:10.1016/j.catena.2007.03.008.

Moody, JA, Smith JD, Ragan BW. 2005. Critical shear stress for erosion of cohesive soils subjected to temperatures typical of wildfires. *Journal of Geophysical Research* **110**(F01004): 1–13. DOI:10.1029/ 2004JF000141.

Moriasi DN, Arnold JG, Van Liew MW, Bingner RL, Harmel RD, Veith TL. 2007. Model evaluation guideline for systematic quantification of accuracy in watershed simulations. *Transactions of the American Society of Agricultural and Biological Engineers* **50**(3): 885–900.

Nash JE, Sutcliffe JV. 1970. River flow forecasting through conceptual models part I - A discussion of principles. *Journal of Hydrology* **10**(3): 282–290.

Nearing MA. 2000. Evaluating Soil erosion models using measured plot data: accounting for variability in the data. *Earth Surface Processes Landforms* **25**: 1035–1043.

Nearing MA, Norton LD, Bulgakov DA, Larionov GA, West LT, Dontsova KM. 1997. Hydraulics and erosion in eroding rills. *Water Resources Research* **33**: 865–876.

Nearing, MA, Wei H, Stone JJ, Pierson FB, Spaeth KE, Weltz MA, Flanagan DC. 2011 A Rangeland hydrology and erosion model. *Transactions of the American Society of Agricultural and Biological Engineers* **54**(3): 1–8.

Parlange J-Y, Lisle I, Braddock RD, Smith RE. 1982. The three-parameter infiltration equation. *Soil Science* **133**(6): 337–341.

Petersen SL, Stringham TK, Roundy BA. 2009. A process-based application of state-and-transition models: a case study of western juniper (Juniperus occidentalis) encroachment. *Rangeland Ecology & Management* **62**: 186–192.

Pierson FB, Bates JD, Svejcar TJ, Hardegree SP. 2007. Runoff and erosion after cutting western juniper. *Rangeland Ecology & Management* **60**(3): 285–292.

Pierson FB, Moffet CA, Williams CJ, Hardegree SP, Clark PE. 2009. Prescribed-fire effects on rill and interrill runoff and erosion in a mountainous sagebrush landscape. *Earth Surface Processes Landforms* **34**: 193–203.

Pierson FB, Robichaud PR, Moffet CA, Spaeth KE, Hardegree SP, Clark PE, Williams CJ. 2008a. Fire effects on rangeland hydrology and erosion in a steep sagebrush-dominated landscape. *Hydrological Processes* **22**: 2916-2929. DOI:10.1002/hyp.6904.

Pierson FB, Robichaud PR, Moffet CA, Spaeth KE, Williams CJ, Hardegree SP, Clark PE. 2008b. Soil water repellency and infiltration in coarse-textured soils of burned and unburned sagebrush ecosystems. *Catena* **74**: 98–108.

Pierson FB, Robichaud PR, Spaeth KE. 2001. Spatial and temporal effects of wildfire on the hydrology of a steep rangeland watershed. *Hydrological Processes* **15**: 2905–2916.

Pierson FB, Williams CJ, Kormos PR., Hardegree SP, Clark PE, Rau BM. 2010. Hydrologic vulnerability of sagebrush steppe following pinyon and juniper encroachment. *Rangeland Ecology & Management* **63**: 614–629.

Pierson FB, Williams CJ, Hardegree SP, Weltz MA, Stone JJ, Clark PE. 2011. Fire, plant invasions, and erosion events on western rangelands. *Rangeland Ecology & Management* **64**: 439–449.

Pierson FB, Williams CJ, Hardegree SP, Clark PE, Kormos PR, Al-Hamdan OZ. 2013. Hydrologic and erosion responses of sagebrush steppe following juniper encroachment, wildfire, and tree-cutting. *Rangeland Ecology & Management* **66**: 274–289.

Robichaud PR. 2000. Fire effects on infiltration rates after prescribed fire in northern Rocky Mountain forests, USA. *Journal of Hydrology* **231-232**: 220–229.

Schlesinger WH, Reynolds JF, Cunningham GL, Huenneke LF, Jarrell WM, Virginia RA, Whitford WG. 1990. Biological feedbacks in global desertification. *Science* **247**(4946): 1043–1048.

Smith RE, Corradini C, Melone F. 1993. Modeling infiltration for multistorm runoff events. *Water Resources Research* **29**(1):133–144.

Smith RE Goodrich DC, Woolhiser DA, Unkrich CL. 1995. Chapter 20: KINEROS: A kinematic runoff and erosion model. In *Computer Models of Watershed Hydrology, 697-732*. Singh VJ (ed.) Water Resources Publications: Highlands Ranch, CO.

Smith RE, Parlange JY. 1978. A parameter-efficient hydrologic infiltration model. *Water Resources Research* **14**(3):533–538.

Spaeth K, Weltz M, Briske DD, Jolley LW, Metz LJ, Rossi C. 2013. Rangeland CEAP: An assessment of natural resources conservation service practices. *Rangelands* **35**(1): 2–10.

Urgeghe AM, Breshears DD, Martens SN, Beeson PC. 2010. Redistribution of runoff among vegetation patch types: On Ecohydrological optimality of herbaceous capture. *Rangeland Ecology & Management* **63**: 497–504.

Wei H, Nearing MA, Stone JJ, Guertin DP, Spaeth KE, Pierson FB, Nichols MH, Moffett CA. 2009. A new splash and sheet erosion equation for rangelands. *Soil Science Society of America Journal* **73**(4): 1386–1392.

Wendt RC, Alberts EE, Hjelmfelt Jr AT. 1986. Variability of runoff and soil loss from fallow experimental plots. *Soil Science Society of America Journal* **50**: 730–736.

Wilcox BP. 2010. Transformative ecosystem change and ecohydrology: Ushering in a new era for watershed management. *Ecohydrology* **3**: 126–130. DOI: 10.1002/eco.104.

Wilcox BP, Pitlick J, Allen CD, Davenport DW. 1996. Runoff and erosion from a rapidly eroding pinyon-juniper hillslope. In *Advances in hillslope processes*, Anderson MG, Brooks SM (eds). Volume 1. John Wiley and Sons, Ltd.: New York, USA; 61–77.

Williams CJ, Pierson FB, Al-Hamdan OZ, Kormos PR, Hardegree SP, Clark PE. 2013. Can wildfire serve as an ecohydrologic threshold-reversal mechanism on juniper-encroached shrublands? *Ecohydrology*. In press. DOI: 10.1002/eco.1364.